



Published in final edited form as:

*Magn Reson Med.* 2005 October ; 54(4): 918–928.

## S<sup>5</sup>FP: Spectrally Selective Suppression with Steady State Free Precession

J. A. Derbyshire<sup>\*</sup>, D. A. Herzka, and E. R. McVeigh

Laboratory of Cardiac Energetics, National Heart, Lung and Blood Institute, National Institutes of Health, DHHS, Bethesda, MD 20892-1061, USA.

### Abstract

A method is presented that employs the inherent spectral selectivity of the Steady-State Free Precession (SSFP) pulse sequence to provide a spectral band of suppression. At  $TE = TR/2$ , SSFP partitions the magnetization into two phase-opposed spectral components. Z-storing one of these components simultaneously further excites the other, which is then suppressed by gradient crushing and RF spoiling. The Spectrally Selective Suppression with SSFP (S<sup>5</sup>FP) method is shown to provide significant attenuation of fat signals, while the water signals are essentially unaffected and provide the normal SSFP contrast. Fat suppression is achieved with relatively little temporal overhead (less than 10% reduction in temporal resolution). S<sup>5</sup>FP was validated using simulations, phantoms, and human studies. Published 2005 Wiley-Liss, Inc.†

### Keywords

MRI; steady-state; balanced SSFP; FISP; fat suppression

Fast imaging with steady precession (FISP) (1) employs balanced steady-state free precession (SSFP) (2), thereby recycling the magnetization, providing a high signal-to-noise ratio (SNR) that is practically independent of the sequence repetition time (TR). We use the term SSFP to refer to the general NMR phenomenon of steady-state free precession, and the term FISP for an SSFP imaging sequence with fully balanced gradients in each TR. Fat, especially in subcutaneous (s.c.) tissues, generates large signals. These can be a source of artifacts, such as Gibbs ringing, and may interfere with the signals of interest by partial volume effects or by obscuring the origin of the signal (e.g., blood). For many practical implementations, the TR of the FISP sequence is such that the contributions of fat to the image are phase opposed to those of water, leading to destructive interference in pixels with partial volumes of water and fat (3). Also, methods requiring a reference image (e.g., SENSE (4)) can be corrupted by large fat signals. Fat surrounding the coronary arteries is also detrimental in coronary artery imaging (CAI) since it can obscure the artery or confound signal from contrast-enhanced blood (5,6). It is, therefore, often desirable to suppress the contribution of fat signals in the image.

Most common fat attenuation methods rely on the differing evolution of water and fat by, for example, frequency or relaxation (5,7-8). They thus require significant evolution time to perform selective suppression and are generally only effective during a limited time-window at a specific delay after application. More recently, methods have been proposed for performing fat suppression or fat/water separations specifically during FISP acquisitions (9-13). These methods require phase-cycling or multiple acquisitions, at least doubling the scan time, and are therefore non-ideal for use with real-time imaging. A single acquisition, phase-based post-

\*Correspondence to: J. A. Derbyshire, Laboratory of Cardiac Energetics, National Heart, Lung and Blood Institute, National Institutes of Health, DHHS, Rm B1D 416, 10 Center Drive, Bethesda, MD 20892-1061, USA. E-mail: jad11@nih.gov

processing method has been proposed (3), but this approach identifies whole voxels as either fat or water and, hence, will suffer from partial volume effects. The benefits and drawbacks of existing methods for water/fat selection in FISP are examined in more detail in the Discussion section.

Here we propose an SSFP-based imaging method that exploits the intrinsic selectivity of SSFP to perform spectral suppression and thereby avoids the need to incorporate additional spectrally selective pulse sequence elements. We refer to this pulse sequence as **Spectrally Selective Suppression with Steady State Free Precession (S<sup>5</sup>FP)**. The scheme is based on breaking the FISP imaging sequence into short trains comprising, for example, 8–64 RF-pulses. At the moment of echo formation ( $TE = TR/2$ ) (3,14) after the last full RF pulse of the train, the water signal is z-stored. Residual transverse magnetization, which comprises isochromats phase-opposed to the on-resonance water, is gradient crushed and RF spoiled. The stored magnetization is subsequently re-excited with little disturbance to the on-resonance steady-state water signal. The additional time required to perform the steady-state interruption is typically as little as a single TR, minimally affecting the efficiency of the imaging process. The sequence can be employed repetitively, greatly reducing the amplitude of fat signals throughout a real-time or cine imaging process.

## THEORY

### Steady State Free Precession: Magnetization Response

It has previously been shown (14) that an SSFP sequence comprising a train of phase-alternated,  $\alpha$ -flip angle RF pulses generates echo signals (similar to spin-echoes) at a time-point  $TE \approx TR/2$  from the midpoints of the RF pulses. Echoes generated under SSFP differ from conventional spin-echoes in that they may be formed with either positive or negative phase depending on the amount of precession experienced in each TR. Isochromats that precess approximately an even number of complete cycles in one TR form an echo in-phase with on-resonance isochromats, while those that precess approximately an odd number of cycles yield signal with opposing phase. That is, echoes from isochromats with off-resonance frequency  $\Delta\omega$  satisfy:

$$\begin{aligned} (2k)2\pi - \pi < \Delta\omega TR < (2k)2\pi + \pi &\Rightarrow \text{positive echo} \\ (2k + 1)2\pi - \pi < \Delta\omega TR < (2k + 1)2\pi + \pi &\Rightarrow \text{negative echo} \end{aligned}$$

where  $k$  is an integer. This effect, shown in Fig. 1 (the SSFP magnetization response function at  $TE = TR/2$ ) allows the isochromats to be separated into two spectral components with a fairly sharp transition zone between the two bands. In this work, this inherent spectral selectivity is exploited to provide water selection and fat suppression, but may be generalized to provide alternate spectral separations. With the scanner center frequency (i.e., 0Hz) set for water, fat (chemical shift = 3.35ppm) has a resonance frequency 214Hz at 1.5T, so any SSFP sequence with  $2.3\text{ms} < TR < 7.0\text{ms}$  will generate an echo at  $t = TR/2$  with fat signals phase-opposed to those from water.

### Spectral Selection: Z-Storing Subsequence

The separation of the isochromats into discrete positive and negatively phased components at TE (see Fig. 2a) provides the opportunity to manipulate the isochromats so as to suppress one component. An  $\alpha/2$  pulse at TE, referred to as the z-storing pulse, is played to rotate the water isochromats to lie along the z-axis (see Fig. 2c) (15). In addition to z-storing the water (or in-phase) isochromats, the pulse also has the effect of further flipping the fat (or phase-opposed) isochromats into the transverse plane so that they have an angle  $\alpha$  with the z-axis. For typical FISP imaging parameters,  $30^\circ < \alpha < 60^\circ$ . The transverse component of the fat is then dephased by gradient crushing, leaving a residual longitudinal component substantially reduced from the normal SSFP steady-state magnitude (see Fig. 2e).

## SSFP Closing Subsequence

We define the angle between the water and fat isochromats just prior to z-storage as the *water-fat separation angle*,  $\zeta$ . As  $\zeta$  is increased toward  $90^\circ$ , the residual longitudinal fat component (after z-storage and gradient crushing) is reduced, resulting in improved suppression. In the simple sequence discussed so far  $\zeta = \alpha$ , the SSFP flip angle, so it is expected that the degree of suppression will increase with flip angle. However, it is generally unfeasible to apply very large flip angles (e.g.,  $\alpha > 60^\circ$ ) for the whole SSFP-train due to limitations on energy deposition and because of undesirable effects on the overall image contrast. An effective water-fat separation angle  $\zeta > \alpha$ , may be achieved by employing a closing subsequence at the end of the SSFP-train comprising  $N_{\text{close}}$  RF pulses with linearly increasing flip angle:

$$\text{flip}[i] = \alpha + \frac{(\zeta - \alpha)}{2N_{\text{close}}}(2i + 1) \quad [1]$$

where  $0 \leq i < N_{\text{close}}$  is the pulse index in the closing subsequence. The subsequence gradually increases the water-fat separation angle from  $\alpha$  to  $\zeta$  in uniform steps. In particular, employing  $\zeta = 90^\circ$  should achieve significantly improved suppression, which theoretically completely crushes the fat magnetization component. The effects of the closing subsequence are illustrated in Fig. 2b,d,f and 8 for  $\zeta = 90^\circ$ .

Data collected during the closing sequence will provide increased signal levels due to the increased transverse component of the magnetization. Defining  $\varphi[i]$  to be the angle between the magnetization and the z-axis after the  $i$ th closing pulse, these data can be re-scaled to normal SSFP signal levels by multiplication by  $\sin(\alpha/2) / \sin(\varphi[i])$ . For example, during SSFP with  $\alpha = 45^\circ$ , the magnetization will lie at an angle  $22.5^\circ$  to the z-axis and water-fat separation of  $45^\circ$ . For  $N_{\text{close}} = 5$  and  $\zeta = 90^\circ$ , we obtain a closing series:

	SSFP		Closing sequence				
pulse index	$\alpha$	0	1	2	3	4	
flip angle	$\pm 45.0^\circ$	$\pm 49.5^\circ$	$\mp 58.5^\circ$	$\pm 67.5^\circ$	$\mp 76.5^\circ$	$\pm 85.5^\circ$	
angle to z-axis: $\varphi$	$22.5^\circ$	$27^\circ$	$31.5^\circ$	$36^\circ$	$40.5^\circ$	$45^\circ$	
water-fat angle: $\zeta$	$45^\circ$	$54^\circ$	$63^\circ$	$72^\circ$	$81^\circ$	$90^\circ$	

followed by a  $\zeta/2 = 45^\circ$  pulse played at the echo time that z-stores the water and fully excites the fat magnetization.

## SSFP Opening Subsequence

While the fat isochromats have been suppressed, the water isochromats, which were stored along the longitudinal axis, have a magnitude that is essentially unaffected by the closing sequence apart from a small amount of  $T^1$  relaxation. In restarting the SSFP-train, the opening subsequence must rapidly separate the spectral components into in-phase and phase-opposed echoes without incurring a lengthy transient period.

An  $(\alpha/2\text{-TR}/2)$  combination (7,15) is often used to restart SSFP sequences that have been interrupted to perform explicit magnetization preparation, for example, tagging (16). However, this opening subsequence generates undesirable transient behavior from isochromats in the off-resonant bands, such as the fat in the present discussion (17). Even though signal from fat has been greatly suppressed in this application, it may still be advantageous to start with a sequence with a smooth transition to steady-state. Opening subsequences employing a linearly ramped flip angle and full TR RF pulse separations have been proposed (17-19) to provide a rapid separation of the fat and water components into phase-opposed echoes at TE. These are particularly effective here as the fat isochromats have recently been nulled and are growing back from very small magnitude. Excellent results are obtained using as few as  $N_{\text{open}} = 5$  RF pulses:

$$\text{flip} = \frac{\alpha}{2N_{\text{open}}}(2i + 1) \quad [2]$$

which linearly increases the angle of the magnetization from the z-axis. Data acquisition can begin with the first RF pulse and, similarly to the closing subsequence, be rescaled to account for the use of lower excitation angles by multiplication by  $\sin(\alpha/2)/\sin(\varphi[i])$ , where  $\varphi[i]$  is the angle subtended by the magnetization to the z-axis after the  $i$ th opening pulse. For the opening subsequence given in Eq. [2]:

$$\varphi[i] = \left| \sum_{k=0}^{i-1} (-1)^k \frac{\alpha}{2N_{\text{open}}}(2k + 1) \right| = \frac{\alpha}{2N_{\text{open}}}(i + 1) \quad [3]$$

for the subsequence index,  $i = 0, \dots, (N_{\text{open}}-1)$ .

### Inter SSFP-Train RF Spoiling

The incorporation of RF-spoiling between successive SSFP-trains provides further suppression of the unwanted spectral component. Generally, RF spoiling is extremely effective in reducing the coherence of transverse magnetization excited in one block with that in subsequent blocks of the sequence (20-22). The method is implemented by applying a linearly increasing phase increment to the RF transmitter and receiver between successive sequence blocks (typically the phase increment increases by  $117^\circ$  each block (23)). For a conventional gradient echo imaging sequence, a block is one TR of the sequence. For the S<sup>5</sup>FP method, however, one block represents the duration of one train of SSFP pulses, including their opening, closing, and z-storing subsequences. The interval between successive blocks should be less than the  $T_2$  of the component to be suppressed, setting an upper bound on the SSFP-train duration.

The process of performing short SSFP-trains with intervening crushing and spoiling of the unwanted fat spectral component is repeated regularly to suppress re-growth of the fat signal over time. Fig. 3 summarizes the overall concept of the method. Simplistically, considering each whole SSFP-train to be a single repetition unit of the pulse sequence, the effect of the method on fat isochromats can be seen to be similar to that of a conventional RF-spoiled gradient echo sequence with flip angle  $\zeta$  and TR equal to the duration of the entire SSFP-train. Since water isochromats begin and end each train in z-storage, they are immune to the inter-train gradient and RF spoiling, and thus retain the SSFP contrast of FISP. The acquisition and rescaling of data during the opening and closing sequences greatly improves the efficiency of the method, such that the only temporal overheads versus conventional FISP are those required for: SSFP echo formation at TE, the z-storage pulse, and the gradient crushing of residual magnetization, typically amounting to about 1 TR.

## METHODS

### Simulations

Computer simulations were performed to obtain the steady-state magnetization response as a function of off-resonance frequency. The performance of (i) standard SSFP; (ii) S<sup>5</sup>FP with gradient crushing applied between trains but RF spoiling disabled, and (iii) S<sup>5</sup>FP with both gradient crushing and RF spoiling were compared. Multiple isochromats ( $N_{\text{iso}}$ ), each corresponding to a given off-resonance frequency, were tracked as the sequence played out. Individual RF pulses were treated as being hard pulses with instantaneous effect. Gradient crushing was simulated by following multiple ( $N_{\text{crush}}$ ) coherence pathways with precession angles uniformly distributed over  $-\pi \leq \theta < \pi$  and taking the mean over all the coherence pathways as the composite isochromat magnetization (24). Parameters varied for simulation included: (i) RF spoiling phase increment  $0^\circ$  (off) or  $117^\circ$  (on); (ii) the SSFP-train length; (iii) the number of RF pulses to be used for the opening and (iv) closing subsequences; and (v) the

final water-fat angle,  $\zeta$ . Other simulation parameters corresponded to those typically employed in a 256-sample conventional FISP sequence:  $\alpha = 45^\circ$ , TR = 3ms, and relaxation parameters for myocardial muscle (T1/T2 = 880/80ms), arterial blood (T1/T2 = 1200/200ms), and fat (T1/T2 = 250/80ms) at 1.5T. The magnetization response function was measured at TE = TR/2, midway between the centers of the two adjacent RF pulses. To allow the magnetization to reach a steady state, the conventional SSFP sequence response was measured on the 1000th TR. To allow the variation of the response throughout the train to be examined, the S<sup>5</sup>FP response was measured for every TR during the 100th SSFP-train.

## Experimental

Experiments were performed using a 1.5T GE Signa CV/i MRI scanner (GE Medical Systems, Waukesha, WI) equipped with gradients rated for 40mT/m amplitude and 150T/m/s slew rate. For parallel imaging (TSENSE) acquisitions employed in the cardiac studies, data were acquired using an 8-channel cardiac phased array coil (Nova Medical, Wilmington, MA) via an in-house constructed, external 8 channel receiver system (25). Experiments involving human volunteers were conducted with full consent under a protocol approved by the NHLBI institutional review board. The basic imaging pulse sequence was previously developed for efficient, continuous imaging with conventional FISP (26). This sequence was modified to perform S<sup>5</sup>FP imaging using multiple short SSFP-trains as described in the theory section. Sequence options included: the number of TRs in the short-train; the use of a ( $\alpha/2$ -TR/2) or ramped opening subsequence with specified numbers of RF pulses; the use of a ramped closing subsequence of particular length and  $\zeta$  angle; and RF spoiling phase increment  $0^\circ$  (off) or  $117^\circ$  (on). In all cases, data acquisition was performed during both the ramped flip opening and closing subsequences. The additional temporal overhead for performing the sequence was exactly 1 TR per SSFP-train. Data rescaling could optionally be performed during off-line data reconstruction.

## Validation of Simulations

To validate the simulations of the S<sup>5</sup>FP response function, a sealed, 5 mm i.d. NMR tube was filled with 0.8 mM Gd-DTPA doped water and placed parallel to the magnet bore in the MRI system. A range of off-resonance frequencies was created by applying a fixed Z-shim offset. Non-phase encoded 1D-projections providing a frequency response similar to the simulations were obtained using the conventional FISP and S<sup>5</sup>FP sequences. Data were acquired after the system reached steady-state. For the S<sup>5</sup>FP sequence, data were acquired for each TR in the train to allow the variation of the response throughout the train to be examined. The effects of (i) enabling/disabling RF spoiling; and varying (ii) the SSFP-train length; (iii) the number of opening and (iv) closing pulses; and (v) the final water-fat angle,  $\zeta$ , were studied and compared to the simulation results.

## Calf Muscle

Axial images of the calf were obtained to investigate the effects of the choice of train-length and final water-fat angle,  $\zeta$ , on the fat suppression. Images were obtained for conventional FISP and S<sup>5</sup>FP using identical parameters: 1ms,  $\alpha = 45^\circ$  flip angle RF pulses and 256 sample, and  $\pm 125$ kHz receiver bandwidth (RBW) acquisitions with TR = 3.3ms. Opening and closing subsequences comprised 5 RF pulses and 1 RF pulse, respectively, with gradient and RF-spoiling between trains. Images were acquired with 24 cm field-of-view (FOV) and 8 mm slice thickness, with an acquisition matrix of 256  $\times$  240. Various factorizations of the 240 phase encodes permitted S<sup>5</sup>FP images to be formed by interleaving short-trains of different lengths. Signal intensity measurements were made on two separate muscle regions-of-interest (ROIs) and four fat ROIs. Twenty images were acquired sequentially, and the last 10 were averaged

to eliminate the transition into steady-state. Mean and SD for both fat and water signals in the ROIs were recorded.

### Cardiac Study

Ungated time series of cardiac images (similar to real-time imaging) were obtained using FISP and S<sup>5</sup>FP with 8 mm slice thickness and FOVs of 36 × 27 cm (short axis) and 36 × 32.4 cm (long axis).

Identical imaging parameters were employed for both FISP and S<sup>5</sup>FP: 1ms,  $\alpha = 45^\circ$  flip RF pulses and 256 sample, and  $\pm 125$ kHz RBW with TR = 3.2ms. The full raw data matrix for each time-frame was 256 × 96. TSENSE (27) parallel imaging provided acceleration rates  $R = 3$  and  $R = 4$  (i.e., 32 and 24 acquired phase encodes per image) for temporal resolutions of 102ms and 77ms, respectively. Interleaving phase encodes for successive frames provided fully sampled, lower temporal resolution coil maps. For example, the  $R = 3$  acquisition order is: [frame 0] 0, 3, 6, ... ; [frame 1] 1, 4, 7, ... ; [frame 2] 2, 5, 8, ... ; and so forth, with a map being reconstructed from the combined data for frames 0, 1, and 2. Time series of 120 image frames ( $R = 3$ ) or 160 image frames ( $R = 4$ ) were collected for each sequence. For standard FISP imaging, the sequence ran without interruption with frame rates 13.0 fps and 9.8 fps, respectively, corresponding to the temporal resolution. For the S<sup>5</sup>FP sequence, each short-train corresponded exactly to one TSENSE image frame (i.e., 24 or 32 TRs), including subsequences comprising  $N_{\text{open}} = 5$ RF pulses and  $N_{\text{close}} = 1$ RF pulse with final water-fat angle,  $\zeta = 90^\circ$ . Z-storage and RF spoiling required a 1 TR overhead providing frame rates 12.5fps and 9.5fps (i.e., 96% and 97% efficient vs. the FISP sequence), respectively.

## RESULTS

### Simulation Results and Experimental Validation

Fig. 4 shows simulated magnetization responses (i.e.,  $M_{xy}$  at TE = TR/2 as a function of the off-resonance precession angle) for conventional FISP and the proposed S<sup>5</sup>FP sequence, with and without RF spoiling. For the S<sup>5</sup>FP sequence, the response shown is the 12th TR of a 24-pulse train. Approximately on-resonance isochromats with precession frequencies satisfying

$$(2k)2\pi - \pi < \Delta\omega\text{TR} < (2k)2\pi + \pi \quad (k \in \mathbb{Z})$$

have a similar response profile to those of SSFP, whereas isochromats with precession frequencies in the range

$$(2k + 1)2\pi - \pi < \Delta\omega\text{TR} < (2k + 1)2\pi + \pi \quad (k \in \mathbb{Z})$$

are significantly suppressed, with additional suppression being provided by RF spoiling.

Fig. 5 presents simulated and experimental data investigating the effects of RF spoiling and the final water-fat separation angle ( $\zeta$ ). The  $M_{xy}$  response is shown in image format for each TR of a  $\alpha = 45^\circ$  flip-angle, 24 TR length train, including opening and closing subsequences of 5 TRs each, with rescaling of data collected during the closing subsequence. There is remarkably good agreement between simulation results shown (left) and corresponding experimental data (right). The inclusion of RF spoiling in the sequence provided significant additional suppression and also yielded a much smoother response in the stop-band ( $-3\pi < \Delta\omega\text{TR} < -\pi$ ). The use of a closing sequence to increase the water-fat separation angle from  $\alpha = 45^\circ$  to  $\zeta = 90^\circ$  provided further suppression of the unwanted spectral band while leaving the passband ( $-\pi < \Delta\omega\text{TR} < \pi$ ) essentially unaffected.

Fig. 6 presents simulated and experimental results on the choice of opening subsequences. The opening subsequence significantly affects the response data for the entire SSFP-train. Furthermore, a smooth opening sequence is advantageous because the efficiency of the

sequence is directly related to the ability to acquire data during the return to steady-state. Responses are shown for  $\alpha = 45^\circ$ , 24 TR length train with  $\zeta = 90^\circ$ ,  $N_{\text{close}} = 1$  pulse closing subsequence, and RF spoiling between trains. As the opening subsequence length increases, the smoothness of the passband also increases, with little change in the appearance of the stopband. Using  $N_{\text{open}} = 5$  RF pulses provides an excellent response. The traditional  $(\alpha/2\text{-TR}/2)$  catalyzing subsequence (15) is also shown (top) and provides a passband performance similar to the linearly ramped, 3 RF pulse, full-TR method, although the stopband appears to have a greater residual signal level than for any of the full-TR opening subsequences.

Similar correspondence between simulations and experiments was obtained for the various other tests described in the Methods section. The specific number of closing pulses did not appear to have a significant impact on either the effectiveness of the spoiling or the transient behavior during the train. In particular, use of  $\zeta = 90^\circ$ ,  $N_{\text{close}} = 1$  pulse closing sequence ( $\text{flip}_{\text{close}} = (\alpha + \zeta)/2$ ) provided a very similar response to those obtained with as many as 5 closing RF pulses. Using a single closing RF pulse has additional benefits: reduced SAR, reduced exposure to  $T_2$  relaxation, and avoiding the need to rescale the closing sequence data.

### Calf Muscle

Fig. 7 compares a standard FISP image of the calf to  $S^5\text{FP}$  images obtained using 24 TR length SSFP-trains including  $N_{\text{open}} = 5$  and  $N_{\text{close}} = 1$  pulse subsequences with various final water-fat angles,  $\zeta$ . The inherent fat suppression provided by the  $S^5\text{FP}$  sequence is readily apparent in both the s.c. and bone marrow tissues and is seen to increase as  $\zeta$  increases. The muscle and blood tissues are relatively unaffected. Fig. 8 provides signal analyses from ROIs in the images and clearly demonstrates that attenuation of the fatty tissues increases with  $\zeta$ , as predicted by theory. Furthermore, s.c. fat behaves similarly to the bone marrow in this respect, while the water-based muscle tissue signal remains constant, independent of  $\zeta$ . An increased muscle tissue signal level was seen, however, for all the  $S^5\text{FP}$  based images versus that for the FISP image. We speculate that this might be due to the suppression of small phase-opposed signal contributions from fat within the muscle.

Fig. 9 compares standard FISP imaging with the  $S^5\text{FP}$  method with  $N_{\text{open}} = 5$ ,  $N_{\text{close}} = 1$ ,  $\zeta = 90^\circ$  for various  $S^5\text{FP}$  train-lengths. Again, the fat suppression provided by the  $S^5\text{FP}$  sequence is readily apparent and improves as the  $S^5\text{FP}$  train-length decreases. In Fig. 10, ROI signal analyses from the images demonstrate that the attenuation of the fat-tissues improves for shorter pulse trains. The signal level of the water-based muscle tissue remains relatively constant, independent of the train-length, at a slightly elevated signal level to that measured in the conventional FISP image.

### Cardiac Study

Examples of the  $S^5\text{FP}$  method applied to TSENSE rate  $R = 4$  accelerated, ungated, continuous cardiac imaging are shown in Fig. 11. For both the short and long axis image sets, the  $S^5\text{FP}$  images exhibit a significant fat suppression relative to the FISP images. Furthermore, continuous fat suppression was achieved at a constant level throughout the time-series of images. The degree of fat suppression varies spatially due to regional field inhomogeneities throughout the chest cavity. Note that the scanner's standard preparatory autoshim procedure was used for these acquisitions and no other special effort was made to shim the subject.

TSENSE reconstruction errors, visible as ghosting of the chest wall in the conventional FISP images, are still visibly present, but greatly suppressed, in the  $S^5\text{FP}$  acquisitions. The  $S^5\text{FP}$  acquisition improves the TSENSE reconstruction in two ways: fat suppression helps avoid signal nulls in the  $B_1$  reference maps due to fat-water cancellation and also because the fat in the chest wall, which is the predominant artifact source, is itself suppressed.

## DISCUSSION

### Technical Details of the Sequence

The S<sup>5</sup>FP sequence acts approximately as filter with a periodic-in-frequency transfer function that comprises passbands, transition bands, and stopbands of equal width,  $1/(2TR)$ . Here, 180° phase alternations of successive RF pulses (including the z-store pulse) fix the scanner center frequency at the center of a S<sup>5</sup>FP spectral passband. In an alternative implementation, with no RF pulse alternation except a 90° phase shift of the final water storage pulse, the response is shifted so that the scanner center frequency lies in a transition band. The spectral bandwidth selected or rejected by the sequence depends inversely on TR. Ideally, the spectral separation of the S<sup>5</sup>FP passband and stopband would be the same as the fat-water frequency shift, that is, approximately 214Hz at 1.5T (28), corresponding to an ideal TR = 4.7ms, or 428Hz at 3T corresponding to an ideal 2.3ms. In practice, the fat and water spectral peaks may not fall at ideal locations in the S<sup>5</sup>FP response. For a given TR, it is usually advantageous to adjust the scanner center frequency so that the water and fat spectral peaks are placed symmetrically with respect to the transition band within a passband and stopband, respectively.

At 1.5T, fat isochromats are phase opposed to water for  $2.3\text{ms} < TR < 7.0\text{ms}$ —sufficient for high-resolution imaging with up to 3 gradient recalled echo acquisitions with 256 samples and as many as 7 echo acquisitions with 128 samples. TRs in the range  $11.7\text{ms} < TR < 16.4\text{ms}$  should also show fat suppression, but such long TRs are likely to generate off-resonance artifacts. At 3T, fat will be in the phase-opposed band for TRs in the range  $1.2\text{ms} < TR < 3.5\text{ms}$ , and also for  $5.8\text{ms} < TR < 8.2\text{ms}$ , which might be useful for spiral-based FISP sequences.

SSFP-train length is an important parameter for the method, although the duration is of greater importance than the particular number of TRs in the train. The train should be short enough for gradient and RF-spoiling to be effective (i.e., duration  $\leq T_2$  fat) and yet long enough for the SSFP condition to develop well-formed echoes with fat phase-opposed to water before the next closing sequence. Better suppression was achieved when the closing RF pulse was increased toward  $\zeta = 90^\circ$ , although no apparent improvement was found by gradually ramping the flip angle over the last few RF pulses of the train.

The acquisition data during the opening and closing sequences (as described in the Theory section) significantly reduce the overhead of the method to as little as 1 TR, that is, a TR/2 delay until echo formation, the Z-storage RF pulse, and a gradient crusher. Without data rescaling, the variation of the angle between the magnetization and the z-axis would yield a modulation of the acquired data. Data rescaling corrects this, but also affects noise level during the opening and closing sequences. Note that in an interleaved phase encoding scheme, the rescaled data would only affect the high spatial frequencies. The data rescaling method may also be applied to other SSFP sequences employing the linear ramped flip subsequence.

### Applications

The method works extremely well with continuous, ungated, and real-time imaging methods. Depending on the number of phase encoding steps required, each full image dataset can be acquired using just one, or several interleaved, SSFP-trains. This acquisition scheme has also been shown to be useful for TSENSE accelerated imaging (27). Fat suppression is maintained at a continuous level throughout the time-series of images, avoiding the artifacts associated with the fat-recovery that result from the sporadic application of fat saturation pulses.

The S<sup>5</sup>FP method is effective for sequences that repeatedly sample the center of  $k$ -space during the imaging process (e.g., projection reconstruction and spiral imaging). A conventional fat-sat method, which only saturates the fat infrequently, can generate artifacts because fat recovery during subsequent imaging causes amplitude and phase discontinuities near the center of  $k$ -



space. The time-efficiency of  $S^5FP$  allows more frequent application, providing more consistent amplitude and phase from fat signals.

### Comparison with Other Fat Saturation Methods

Most traditional fat suppression methods assume that the water and fat magnetization are not initially distinct, and rely on them evolving differently, either by precessional frequency (chemical-shift) or  $T_1$  relaxation time, to effect suppression. A chemically selective RF pulse is usually of fairly significant duration (typically  $<10ms$  for a 1.5T system), so fat saturation may be performed infrequently, allowing significant fat magnetization re-growth during subsequent imaging. Implementation during FISP also necessitates a lengthy interruption of the SSFP process, requiring additional start-up time to re-establish the SSFP steady state. Inversion pulses can also be employed to null the fat signal, but are only effective at a specific evolution time and cannot be used for continuous suppression.

Methods have recently been proposed for SSFP specific spectral separations. The FEMR (9) and LC-SSFP (10) techniques proposed by Vasanawala use phase-cycling to manipulate the SSFP spectral response into a filter with well-defined pass and stop frequency bands. For suitable TRs, water and fat can be placed into the appropriate bands, providing spectrally selective images. Hardy and coworkers (11) propose similar schemes based on cycling the RF flip angle. Overall and colleagues (12) provide a generalized approach based on the Shinnar–Le Roux algorithm for methods based on periodic cycling of RF amplitude and phase. The multi-point Dixon method for FISP, recently proposed by Reeder and colleagues (13), is based on acquiring data at 3 or more TEs. It provides a fat-water separation method that is robust to  $B_0$  inhomogeneities, but requires an extended TR, which may itself be an artifact source. The main drawback of these methods is that the imaging time is increased by the order of the phase-cycling scheme, with a corresponding loss of temporal resolution and/or increased scanning time.

Hargreaves (3) proposed a method for fat-water separation that requires no additional overhead; it simply labels voxels as fat if they are *negative* in a phase-sensitively reconstructed dataset. The method is simple to implement, but suffers the drawback that each voxel is identified as being either wholly water or fat. The issue of how to assign voxels containing partial volumes of water and fat and the problems caused by destructive interference and resulting signal dropout remain.

Recently, Santos and coworkers (8) proposed a method for continuous fat saturation with real-time SSFP imaging, which also employs short SSFP-trains. However, that method attempts to z-store both components of the magnetization at the end of the train by playing an  $\alpha/2$  pulse after a full TR, that is, relinquishing the inherent spectral selection provided by the SSFP. Instead, spectral selection is then achieved using an explicit  $(+90^\circ)$ -TE- $(-90^\circ)$  combination to impart a sinusoidal weighting in  $M_z$  according to the resonant offset frequency, repeated inversions causing saturation of the unwanted spectral component. In contrast,  $S^5FP$  exploits the inherent spectral selection of the SSFP sequence to select the spectral band for spoiling. Nonetheless, these two methods may be combined by simply inserting a  $(+90^\circ)$ -TE- $(-90^\circ)$  sequence between the SSFP-trains, possibly providing additional suppression, at the expense of increased interruption to the SSFP sequence.

The  $S^5FP$  method suppresses magnetization in particular off-resonance frequency bands. For the purposes of fat suppression, off-resonance is assumed to be caused by chemical shift. The sequence does not distinguish between chemical shift and off-resonance from other sources, such as  $B_0$  inhomogeneities. In this respect, it is similar to the majority of fat suppression methods relying on chemical shift for selection or suppression including: conventional chem-sat pulses, the LC-SSFP and FEMR methods, the phase-sensitive SSFP reconstruction method,

and the real-time method of Santos. Furthermore, the frequency pass- and stopbands generated by the  $S^5FP$ , LC-SSFP, FEMR, and phase sensitive SSFP methods are directly related to the SSFP TR parameter, which may require some tuning for various  $B_0$  field strengths. In contrast, the multi-point Dixon method, while chemical-shift based, avoids this inhomogeneity problem by implicitly measuring the local field inhomogeneity as part of the imaging process.

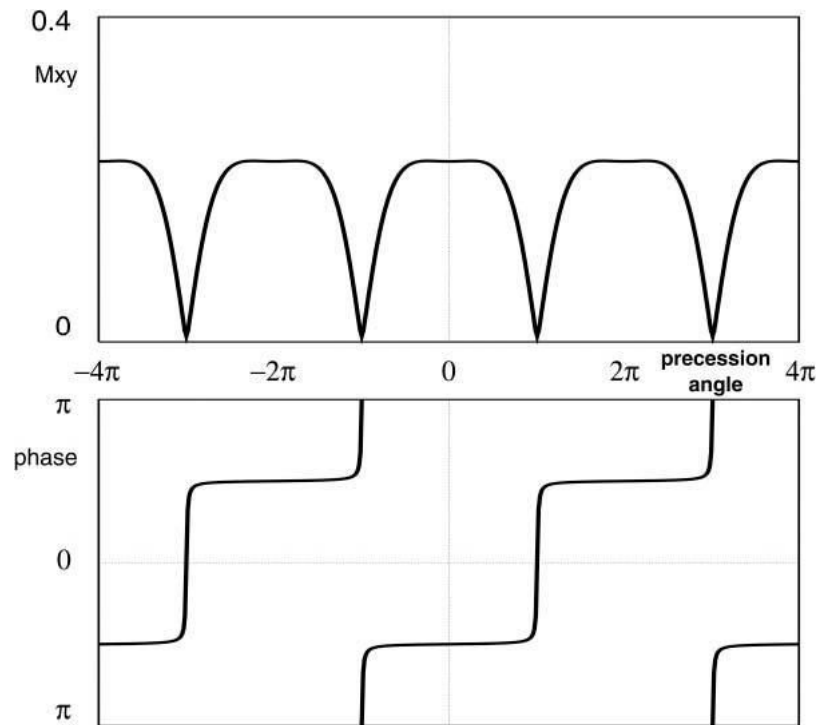
## CONCLUSIONS

We have demonstrated a simple modification to the FISP imaging sequence that efficiently provides fat-suppression while avoiding a lengthy interruption in the SSFP steady state for an explicit fat-saturation sequence. In particular, it was shown that the SSFP sequence underpinning FISP partitions the magnetization into two spectral groups (i.e., positive and negatively phased echoes) at the  $TE = TR/2$  time-point. For common imaging TRs, water and fat fall into different groups, permitting an efficient fat suppression and avoiding the need for an additional evolution time to separate the species.  $S^5FP$  provides effective suppression of a range of frequencies of bandwidth  $1/TR$  adjacent to a passband of approximately the same size. The method is robust and straightforward to implement on 1.5T scanners and should also be applicable at 3T.

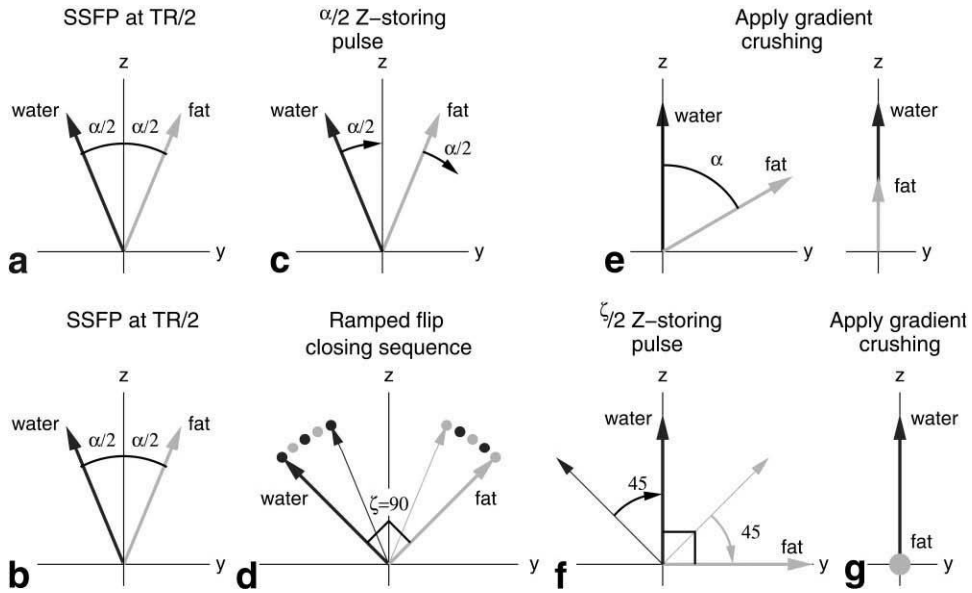
## REFERENCES

1. Oppelt A, Graumann R, Barfuss H, Fischer H, Hartl W, Schajor W. FISP—a new fast MRI sequence. *Electromedica* 1986;54(1):15–18.
2. Carr HY. Steady-state free precession in nuclear magnetic resonance. *Phys Rev* 1958;112:1693–1701.
3. Hargreaves BA, Vasanawala SS, Nayak KS, Hu BS, Nishimura DG. Fat-suppressed steady-state free precession imaging using phase detection. *Magn Reson Med* 2003;50:210–213. [PubMed: 12815698]
4. Pruessmann KP, Weiger M, Scheidegger MB, Boesiger P. SENSE: Sensitivity encoding for fast MRI. *Magn Reson Med* 1999;42:952–962. [PubMed: 10542355]
5. Deshpande VS, Shea SM, Laub G, Simonetti OP, Finn JP, Li D. 3D magnetization-prepared True-FISP: A new technique for imaging coronary arteries. *Magn Reson Med* 2001;46:494–502. [PubMed: 11550241]
6. Flamm SD, Muthupillai R. Coronary artery magnetic resonance angiography. *J Magn Reson Imag* 2004;19:686–709.
7. Scheffler K, Heid O, Hennig J. Magnetization preparation during the steady state: Fat-saturated 3D TrueFISP. *Magn Reson Med* 2001;45:1075–1080. [PubMed: 11378886]
8. Santos, JA.; Hargreaves, BA.; Nayak, KS.; Pauly, JM. Real-time fat suppressed SSFP; Proceedings 11th Annual Meeting ISMRM; Toronto, Canada. 2003. p. 982
9. Vasanawala S, Pauly J, Nishimura D. Fluctuating equilibrium MRI. *Magn Reson Med* 1999;42:876–883. [PubMed: 10542345]
10. Vasanawala SS, Pauly JM, Nishimura DG. Linear combination steady-state free precession MRI. *Magn Reson Med* 2000;43:82–90. [PubMed: 10642734]
11. Hardy, CJ.; Dixon, WT. Steady-state precession imaging with inherent fat suppression; Proceedings 10th Annual Meeting ISMRM; Honolulu, Hawaii, USA. 2002. p. 473
12. Overall WR, Nishimura DG, Hu BS. Steady-state sequence synthesis and its application to efficient fat-suppressed imaging. *Magn Reson Med* 2003;50:550–559. [PubMed: 12939763]
13. Reeder SB, Wen Z, Yu H, Pineda AR, Gold GE, Markl M, Pelc NJ. Multicoil Dixon chemical species separation with an iterative least-squares estimation method. *Magn Reson Med* 2004;51:35–45. [PubMed: 14705043]
14. Scheffler K, Hennig J. Is TrueFISP a gradient-echo or a spin-echo sequence? *Magn Reson Med* 2003;49(2):395–397. [PubMed: 12541263]
15. Deimling, M.; Heid, O. Magnetization prepared true FISP imaging; Proceedings 2nd Annual Meeting SMRM; San Francisco, California, USA. 1994. p. 495

16. Herzka DA, Guttman MA, McVeigh ER. Myocardial tagging with SSFP. *Magn Reson Med* 2003;49:329–340. [PubMed: 12541254]
17. Hennig J, Speck O, Scheffler K. Optimization of signal behavior in the transition to driven equilibrium in steady-state free precession sequences. *Magn Reson Med* 2002;48(5):801–809. [PubMed: 12417994]
18. Zwanenburg JJM, Kuijter JPA, Marcus JT, Heethaar RM. Steady-state free precession with myocardial tagging: CSPAMM in a single breath-hold. *Magn Reson Med* 2003;49:722–730. [PubMed: 12652544]
19. Deshpande V, Chung Y, Zhang Q, Shea S, Li D. Reduction of transient signal oscillations in True-FISP using a linear flip angle series magnetization preparation. *Magn Reson Med* 2003;49(1):151–157. [PubMed: 12509831]
20. Zur, Y.; Bendel, P. Elimination of the steady-state transverse magnetization in short TR imaging; Proceedings 6th Annual Meeting SMRM; New York, New York, USA. 1987. p. 440
21. Crawley AP, Wood ML, Henkelman RM. Elimination of transverse coherences in FLASH MRI. *Magn Reson Med* 1988;8:248–260. [PubMed: 3205155]
22. Darrasse, L.; Mao, L.; Saint-James, H. Spoiling techniques in very fast TR imaging; Proceedings 7th annual meeting SMRM; San Francisco, California, USA. 1988. p. 611
23. Zur Y, Wood ML, Neuringer LJ. Spoiling of transverse magnetization in steady-state sequences. *Magn Reson Med* 1991;21:251–263. [PubMed: 1745124]
24. Sekihara K. Steady-state magnetizations in rapid NMR imaging using small flip angles and short repetition intervals. *IEEE Trans Med Imag* 1987;6(2):157–164.
25. Morris, HD.; Derbyshire, JA.; Kellman, P.; Chesnick, AS.; Guttman, MA.; McVeigh, ER. A wide-band multi-channel digital receiver and real-time reconstruction engine for use with a clinical MR scanner; Proceedings 10th Annual Meeting ISMRM; Honolulu, Hawaii, USA. 2002. p. 61
26. Derbyshire, JA.; McVeigh, ER. GROMIT: A SSFP imaging sequence employing hardware optimized gradients and just-in-time waveform synthesis; Proceedings 10th Annual Meeting ISMRM; Honolulu, Hawaii, USA. 2002. p. 2359
27. Kellman P, Epstein FH, McVeigh ER. Adaptive sensitivity encoding incorporating temporal filtering (TSENSE). *Magn Reson Med* 2001;45:846–852. [PubMed: 11323811]
28. Haacke, EM.; Brown, RW.; Thompson, MR.; Venkatesan, R. Wiley; New York: 1999. Magnetic resonance imaging: physical principles and sequence design.



**FIG 1.** Simulated SSFP magnetization response measured at  $TE = TR/2$  as a function of off-resonance frequency, shown here as the angle an isochromat precesses in  $TR$ , that is,  $\theta = \Delta\omega TR$ . Simulated parameters:  $T1/T2 = 500/100\text{ms}$ ,  $TR = 3.0\text{ms}$ , and flip angle  $\alpha = 45^\circ$ , with  $180^\circ$  phase-cycling between RF pulses. The magnitude response is partitioned into bands; the phase within each band is essentially constant, representing the formation of an echo signal. Note, however, that adjacent bands are phase shifted by  $\pi$  radians; thus, the echo signals from adjacent bands are phase-opposed.

**FIG 2.**

A YZ-plane view of water and fat isochromats demonstrating the fat suppression mechanism. In the upper figures, (a) shows the relative positions of magnetization at the TR/2 echo time-point. In (c), the water magnetization is z-stored by application of the  $\alpha/2$  RF pulse. After gradient crushing (e), the fat component is reduced in effective size. The lower figure demonstrate improved fat suppression using a linear ramped closing sequence that increases the angle between the fat and water isochromats to  $\zeta = 90^\circ$ . In (b) the relative positions of magnetization at the TR/2 echo time are shown. (d) depicts the closing sequence, linearly increasing the effective water-fat separation angle from  $\alpha$  to  $\zeta$  in 4 TRs. In (f), the  $\zeta/2$  RF pulse is applied to effect z-storage of the water magnetization. Finally, in (g), spoiling of the transverse magnetization reduces the effective size of the fat component.

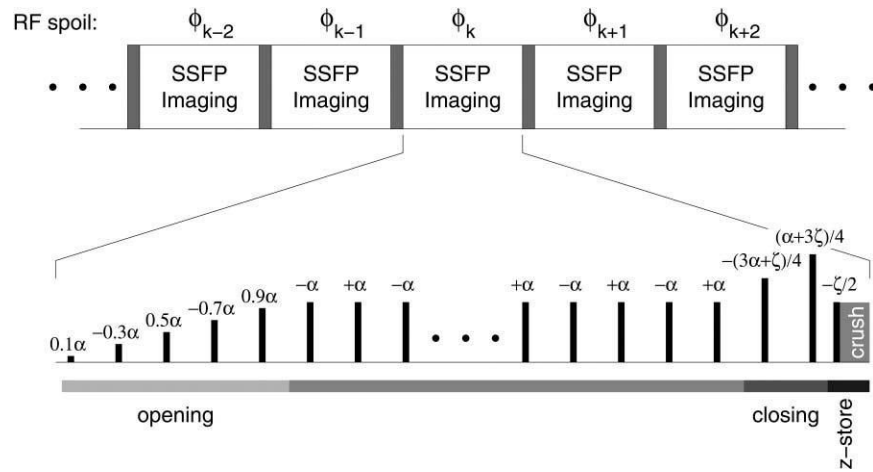


**FIG 3.** Overview of the S<sup>5</sup>FP sequence, depicted here with  $N_{\text{open}} = 5$  and  $N_{\text{close}} = 2$  RF pulses. The RF transmitter and receiver phase for a given short train relative to the preceding one is determined by standard RF spoiling methods, that is,  $\phi_k = \phi_{k-1} + k\theta_{\text{spoil}}$ .

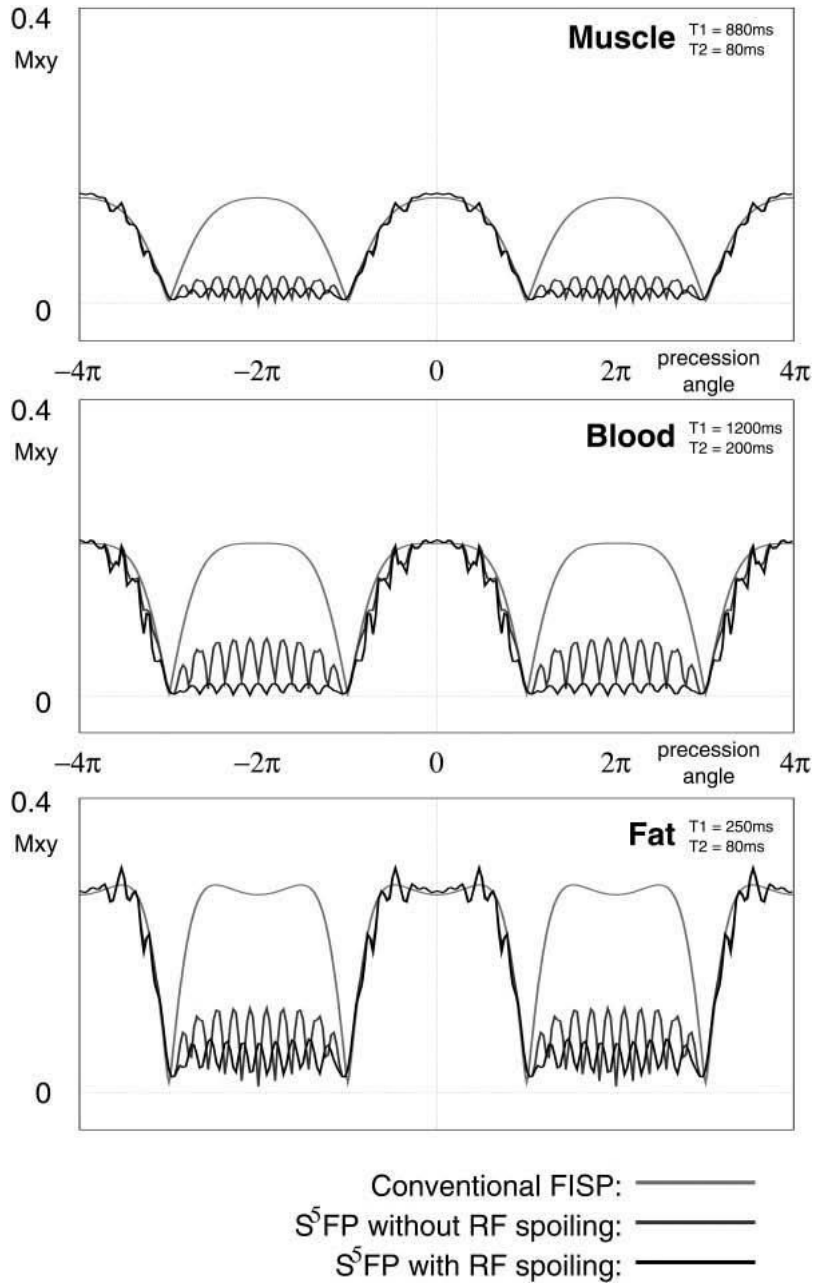


**FIG 4.** Simulated magnetization responses as a function of off-resonance frequency (shown as the precession angle per TR) for muscle (top), blood (center), and fat (lower) tissues to (i) a conventional FISP sequence, (ii)  $S^5FP$  without RF spoiling, and (iii) a full  $S^5FP$  sequence with gradient crushing and RF spoiling. In all cases, the TR was simulated as 3ms and  $\alpha = 45^\circ$  flip angle. Each  $S^5FP$  train used 5 RF pulses for opening and closing subsequences, ramping from  $0^\circ$  to  $\alpha$  and from  $\alpha$  to  $\zeta = 90^\circ$ , respectively.

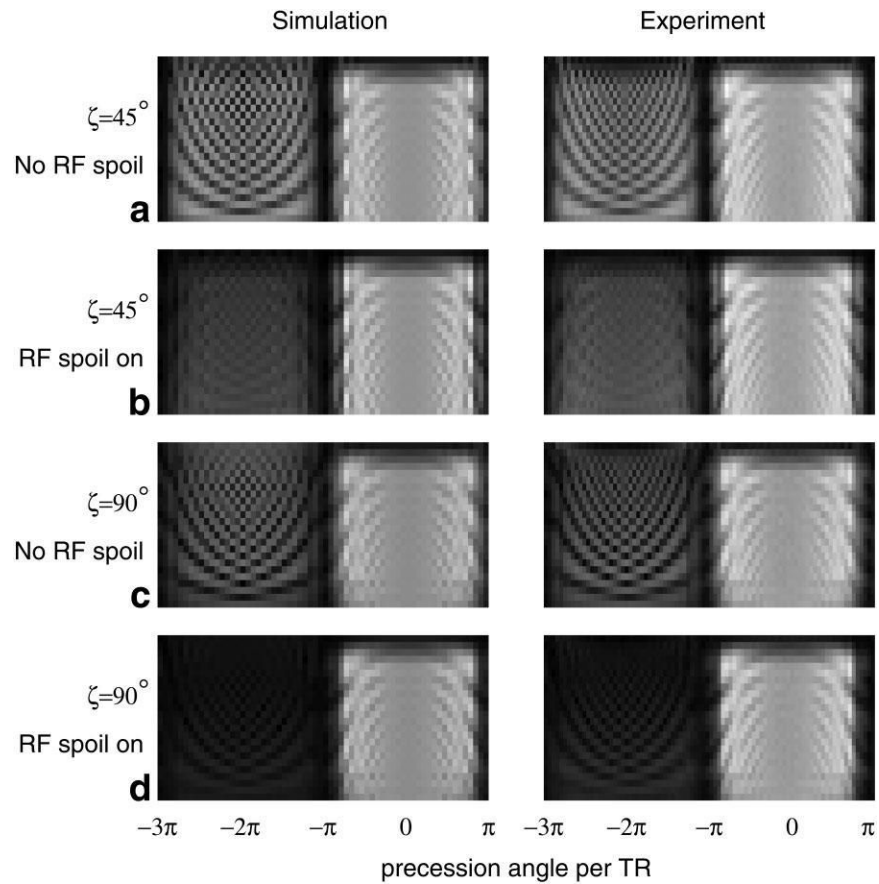


**FIG 5.** Investigation of the benefits of RF spoiling for  $S^5FP$ . Each row of data (from top to bottom) within an image represents the  $M_{xy}$  response for successive TRs to a 24 TR length  $S^5FP$  train. Simulated response data are shown in the left column with experimental data in the right. Top to bottom are shown: (1)  $\alpha = \zeta = 45^\circ$  without RF spoiling between trains; (2)  $\alpha = \zeta = 45^\circ$  with RF spoiling; (3)  $\alpha = 45^\circ$ ,  $\zeta = 90^\circ$  without RF spoiling; (4)  $\alpha = 45^\circ$ ,  $\zeta = 90^\circ$  with RF spoiling.



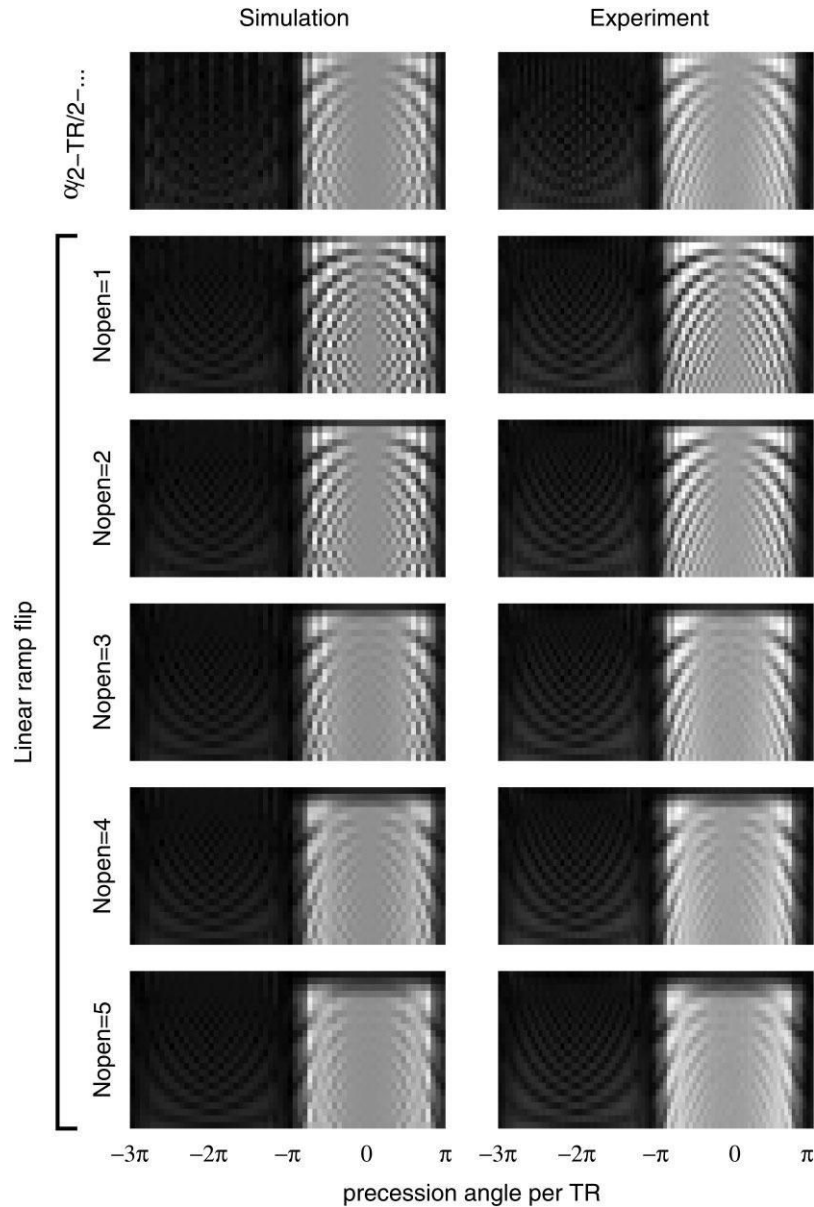


**FIG 6.** Investigation of the effects of opening subsequence for  $S^5FP$ . Each row of data within an image represents the  $M_{xy}$  response in successive TRs to a 24 TR length  $S^5FP$  train obtained with flip angle  $45^\circ$ ,  $\zeta = 90^\circ$ ,  $N_{close} = 1$ , and RF spoiling enabled. There is excellent agreement between simulation (left) and experimental data (right). Top to bottom are shown: (1) the response to the conventional  $\alpha/2-TR/2$  sequence, (2)–(6) the response to a linearly ramped flip angle open subsequence of  $N_{open} = 1-5$  RF pulses, respectively. Data acquired during the opening subsequences are shown in the first few TRs of each plot without rescaling. As expected, the smoothness of the passband improves with longer opening subsequences, and there is little change in the appearance of the stopband. Note also that the conventional  $\alpha/2-TR/2$  opening sequence gives a passband response approximately as smooth as the  $N_{open} = 3$  sequence, but with slightly higher residual signal artifact in the stopband.

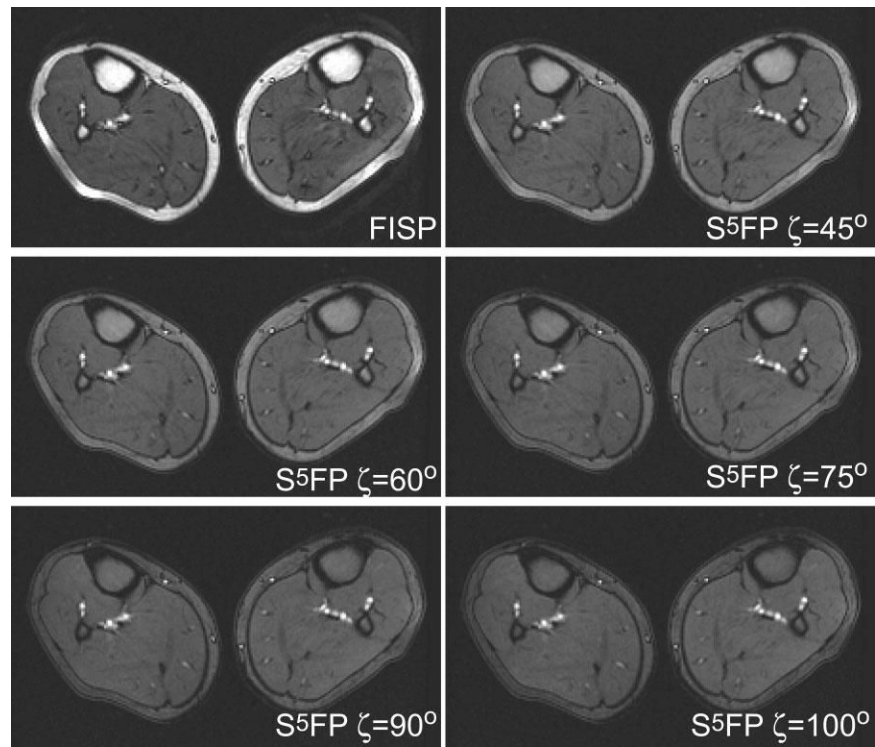


**FIG 7.** Comparison of calf images acquired using conventional FISP and  $S^5FP$  pulse sequences with various water-fat separation angles,  $\zeta$ . The  $S^5FP$  images employed a train length of 24 TRs, including opening and closing subsequences of 5 pulses and 1 pulse, respectively, and RF spoiling between successive SSFP trains.

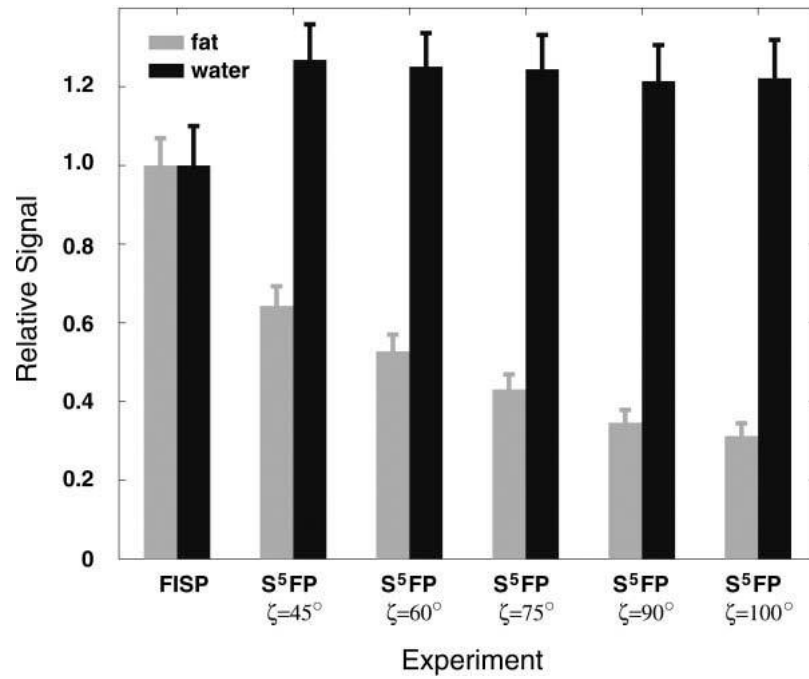


**FIG 8.** Comparison of signal levels from ROIs in the calf images displayed in Fig. 7, comprising fat and water based tissue types acquired using conventional FISP and S<sup>5</sup>FP pulse sequences for various values of water-fat separation angle,  $\zeta$ .

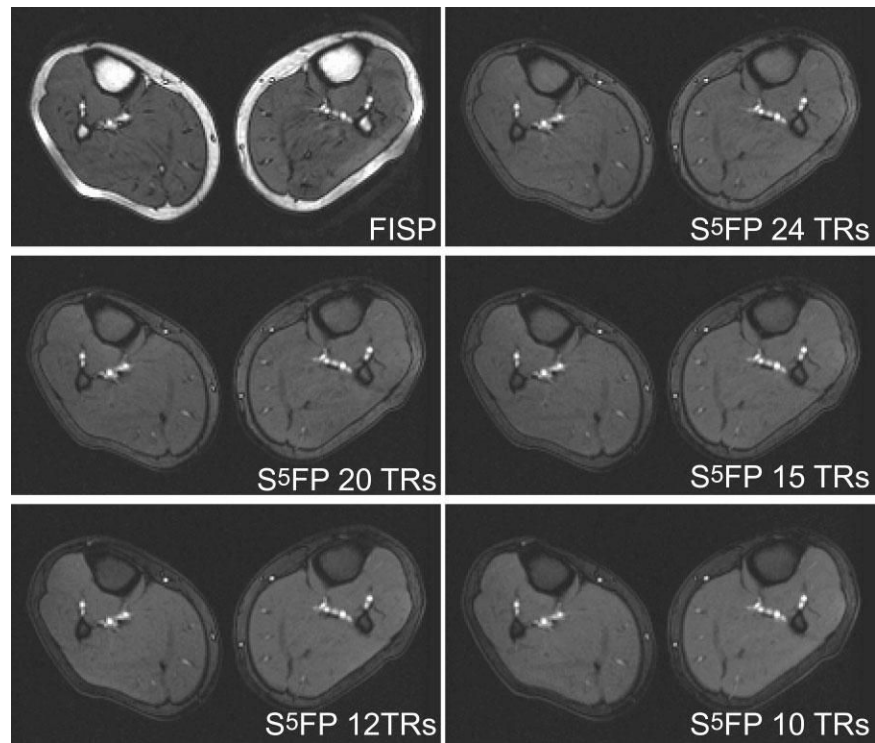


**FIG 9.** Comparison of images of calf acquired using conventional FISP and S<sup>5</sup>FP pulse sequences with various train-lengths. The S<sup>5</sup>FP images employed opening and closing subsequences of 5 pulses and 1 pulse, respectively, a water-fat separation angle of 90°, and RF spoiling between successive SSFP trains.

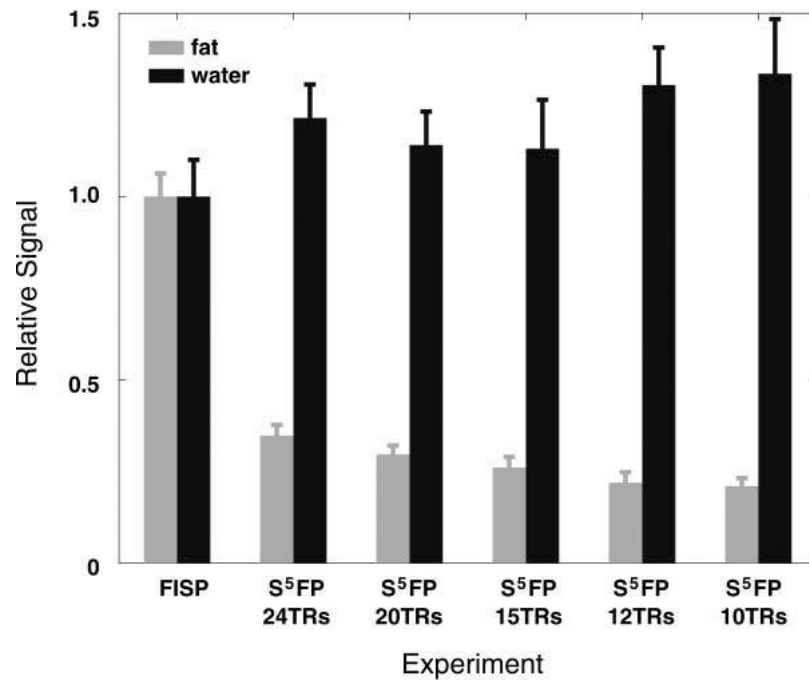


**FIG 10.** Comparison of signal levels from ROIs in the calf images displayed in Fig. 9, comprising fat and water based tissue types acquired using conventional FISP and S<sup>5</sup>FP pulse sequences with various durations for the short-train sequence.

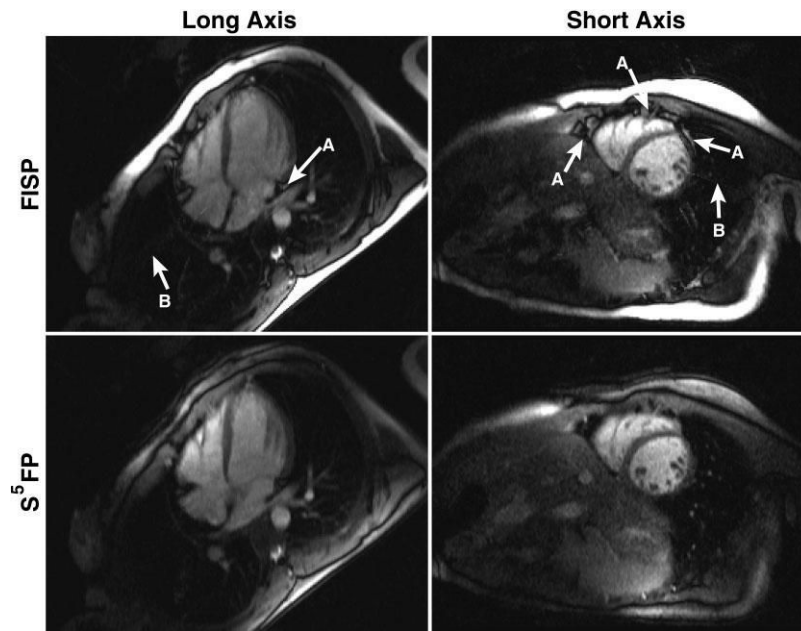


**FIG 11.** Comparison of cardiac images acquired using conventional FISP (top) and S<sup>5</sup>FP (bottom). Although there is some variation in the fat signal level due to field non-uniformity, significant fat suppression is seen throughout the S<sup>5</sup>FP images. In particular, excellent suppression was achieved for pericardial fat in the regions labeled “A.” Artifacts from imperfect TSENSE reconstruction labeled “B” in the FISP image are much reduced in the S<sup>5</sup>FP images.